energy&fuels

Article

pubs.acs.org/EF

Assessment of the Thermophysical Properties of Thermally Stressed RP-1 and RP-2

Tara J. Fortin* and Thomas J. Bruno

National Institute of Standards and Technology, Material Measurement Laboratory, Applied Chemicals and Materials Division, 325 Broadway MS 647.07, Boulder, Colorado 80305, United States

ABSTRACT: Density, speed of sound, and viscosity have been measured for samples of RP-1 and RP-2 that were stressed for 0.5 min at 475 and 510 °C at a pressure of 17 MPa. Density and speed of sound were measured from 5 to 50 °C for samples stressed at 475 °C and from 5 to 35 °C for samples stressed at 510 °C. Viscosity was measured from −10 to 50 and 35 °C for the samples stressed at 475 and 510 °C, respectively. All measurements were made at ambient atmospheric pressure (~83 kPa). Additionally, the density and sound speed data were used to derive adiabatic compressibilities, and those results have also been included. Current results for the thermally stressed samples were compared to previously reported measurement results for unstressed RP-1 and RP-2. For all reported properties, increased thermal stressing resulted in increased fuel decomposition and increased deviations from unstressed values.

1. INTRODUCTION

A liquid propellant rocket engine (LPRE) generates thrust by converting propellant chemical energy into kinetic energy. Conversion occurs when propellants are introduced into the engine combustion chamber where they are burned to form hot gas; the hot gas is then expanded and accelerated through a supersonic nozzle to provide thrust. In a bipropellant LPRE, the propellants include an oxidizer and a fuel. Although an estimated 170 different fuels have undergone laboratory evaluations as potential liquid propellants, certain propellant combinations have proven themselves to be most useful in U.S. space applications, including the combination of liquid oxygen (LOX) oxidizer and kerosene fuel.[1,2]

Conditions in a typical LPRE combustion chamber are extreme, with pressures ranging from 1 to 26 MPa and temperatures ranging from approximately 1727 to 3627 °C.[3] Because these elevated temperatures exceed known material limits, efficient cooling of the thrust chamber has historically been a critical engineering challenge.[1] A variety of cooling techniques have been employed, but one of the more common methods is regenerative cooling,[1] which was first postulated by Konstantin Tsiolkovsky in 1903.[4] With regenerative cooling, one of the precombustion propellants, typically the fuel, is circulated through channels in the thrust chamber wall to carry heat away. With hydrocarbon fuels such as kerosene, the extreme heat absorbed by the fuel during the cooling process can result in molecular decomposition and deposition of insoluble products on the cooling channel walls. This process, referred to as "fouling" or "coking", can result in material failure or "burn out" since the deposits act as a thermal barrier, subsequently increasing the wall temperature of the combustion chamber. Additionally, changes in the fuel's properties as a result of thermal decomposition can ultimately affect fuel performance. Thus, knowledge of the fuel's thermal stability is vital.

Since its development in the mid-1950s, rocket propellant 1 (RP-1) has been commonly used as the kerosene fuel in U.S. space applications.[2] Compared to common jet fuels, which had been previously utilized, current RP-1 specifications allow for a narrower density range and lower concentrations of certain fuel components thought to cause deposits during regenerative cooling (e.g., sulfur, olefins, and aromatics).[1] Specifically, density is only allowed to vary from 0.799 to 0.815 g/cm^3, and the maximum allowed sulfur, olefin, and aromatic concentrations are limited to 30 mg/kg, 2.0% vol/vol, and 5.0% vol/vol, respectively.[5] Additional reformulations of RP-1 aimed at further limiting the concentrations of those components responsible for deposit formation and metal corrosion ultimately resulted in the development of RP-2. While most specifications for RP-1 and RP-2 are identical, the maximum allowed sulfur and olefin concentrations for RP-2 are limited to 0.1 mg/kg and 1.0% vol/vol, respectively.[5]

The thermal stabilities of RP-1 and, to a lesser extent, RP-2 have been thoroughly studied, particularly with respect to the conditions that lead to coking.[6−28] Studies of how thermal stressing affects the thermophysical properties of RP-1 and RP-2 are lacking, however. In an effort to address this disparity, a comprehensive study was undertaken at the National Institute of Standards and Technology (NIST). As part of that study, Windom and Bruno[29] recently reported their assessment of the volatility of thermally stressed RP-1 and RP-2 as determined by the advanced distillation curve method. In this paper, measurements made at ambient pressure of the thermophysical properties density, speed of sound, and viscosity, and the derived property adiabatic compressibility, are reported for the same thermally stressed RP-1 and RP-2 fuel samples.

2. MATERIALS AND METHODS

2.1. Rocket Propellant Samples. A sample of RP-1, designated RP-1-4572, was obtained from the Air Force Research Laboratory Propulsion Directorate at Wright Patterson Air Force Base. This sample was pink in color due to the presence of the dye additive azobenzene-4-azo-2-naphthol. A sample of RP-2, designated RP-2-

Received: January 31, 2013
Published: May 2, 2013

dx.doi.org/10.1021/ef400193d | Energy Fuels 2013, 27, 2506−2514

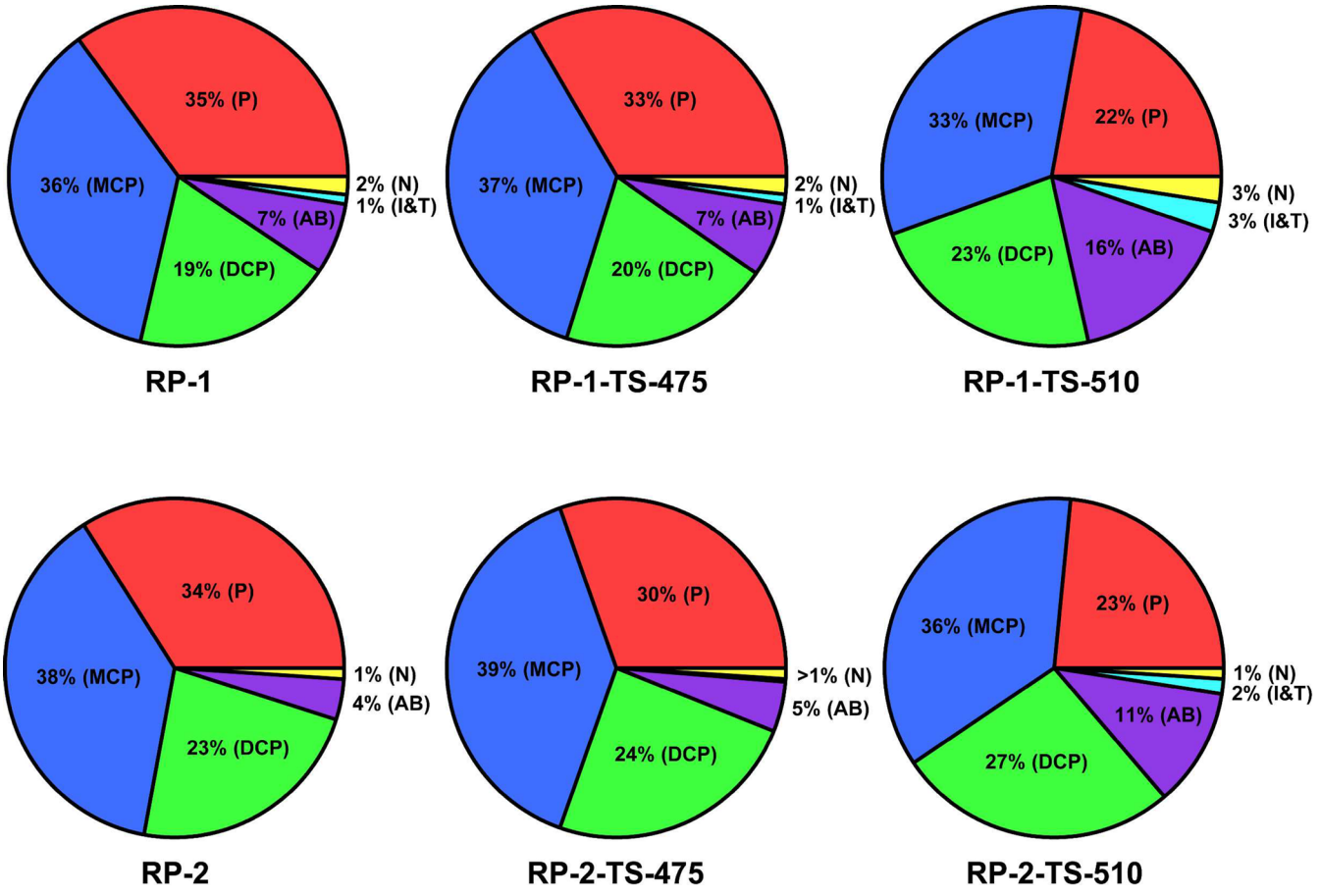

Figure 1. Schematic representation of the hydrocarbon classification analysis of unstressed and thermally stressed RP-1 and RP-2 samples.[29] Analysis is based on ASTM Method D-2789,[36] and it classifies hydrocarbon samples into six families: paraffins (P), monocycloparaffins (MCP), dicycloparaffins (DCP), alkylbenzenes (AB), indanes and tetralins (I&T), and naphthalenes (N). Numbers shown represent the measured percent volume fraction for each of the six families.

EAFB, was obtained from Edwards Air Force Base. In accordance with fuel specifications for RP-2[5], this sample did not contain a dye additive and was therefore colorless. Both of these samples have previously been the focus of extensive research efforts, which included measurements of their composition and their thermophysical and transport properties and culminated in the development of a surrogate mixture model for each fuel.[30−34] Detailed chemical composition information has been published elsewhere,[30,31,35] but in general, the two unstressed fuels had compositions that were typical of kerosenes, composed primarily of alkanes (or paraffins) and containing a small amount of aromatics.

Additional comparisons of the unstressed fuels can be made with the aid of a hydrocarbon classification method based on ASTM Method D-2789.[36] With this method, mass spectral fragments are used to classify hydrocarbon samples into six different types or families: paraffins (P), monocycloparaffins (MCP), dicycloparaffins (DCP), alkylbenzenes (AB), indanes and tetralins (I&T), and naphthalenes (N). Although this method is only specified for use with low-olefinic gasoline samples and has several limitations and sources of uncertainty,[37] it is routinely used for a variety of fuels and provides a convenient basis for fuel-to-fuel comparisons. Results of the hydrocarbon classification for unstressed RP-1 and RP-2 reported by Windom and Bruno[29] are represented schematically in Figure 1. Linear and branched paraffins collectively accounted for approximately 35% and 34% (vol/vol) of the total composition for RP-1 and RP-2, respectively. Additionally, both samples contained a significant number of cycloparaffins; monocycloparaffins accounted for approximately 36% and 38% (vol/vol) and dicycloparaffins accounted for approximately 19% and 23% (vol/vol) of the total composition for RP-1 and RP-2, respectively.[29] It is clear from the preceding information that RP-1 and RP-2 are quite similar in their composition. The primary difference between the two is in their respective sulfur content; fuel specifications allow for a maximum of 30 ppm (mass/mass) total sulfur for RP-1 but a maximum of only 100 ppb (mass/mass) total sulfur for RP-2.[5] The secondary difference between the two is in their respective aromatic content; even though fuel specifications allow for the same maximum volume percent of aromatics,[5] RP-2 was found to have a lower aromatic content than RP-1[29] (Figure 1).

The reactor that was built to thermally stress the fuels has been described in detail elsewhere.[29,38] Briefly, the fuel is pressurized by use of a high-pressure syringe pump and then delivered to a high-temperature reactor capable of generating controlled temperatures up to 600 °C. Downstream of the reactor, the fluid is delivered to a chilled water bath heat exchanger to cool the fluid and quench decomposition reactions. The cooled fluid is then directed through a back-pressure regulator and into a collection vessel. The combination of the syringe pump and back-pressure regulator allows the operator to control the residence time of the fluid in the reactor by providing controlled, constant flow rates at a wide range of nominal pressures. For this work, the RP-1 and RP-2 samples were both thermally stressed for 0.5 (±0.05) min at a constant pressure of 17 (±0.1) MPa and at two temperatures, 475 and 510 °C. Thermally stressed samples will hereafter be designated with a suffix containing "TS" and the stress temperature. Therefore, RP-1-TS-475 refers to the sample of RP-1 thermally stressed at 475 °C.

The chemical composition of the thermally stressed samples was previously analyzed using gas chromatography−mass spectrometry (GC-MS),[39,40] and the results were reported by Windom and Bruno.[29] The results of their hydrocarbon classification analysis for the four

dx.doi.org/10.1021/ef400193d | Energy Fuels 2013, 27, 2506−2514

Table 1. Measured Densities and Speeds of Sound and Derived Adiabatic Compressibilities for Thermally Stressed RP-1 at Ambient Pressure[a]

	RP-1-TS-475						RP-1-TS-510					
t (°C)	$\overline{\rho}$ (kg m^{-3})	$U(\overline{\rho})^b$ (kg m^{-3})	$\overline{w}$ (m s^{-1})	$U(\overline{w})^b$ (m s^{-1})	$\overline{\kappa}_s$ (TPa^{-1})	$U(\overline{\kappa}_s)^b$ (TPa^{-1})	$\overline{\rho}$ (kg m^{-3})	$U(\overline{\rho})^b$ (kg m^{-3})	$\overline{w}$ (m s^{-1})	$U(\overline{w})^b$ (m s^{-1})	$\overline{\kappa}_s$ (TPa^{-1})	$U(\overline{\kappa}_s)^b$ (TPa^{-1})
5.00	810.37	0.09	1367.2	0.4	660.1	0.2	810.38	0.40	1342.4	0.8	684.8	0.5
10.00	806.69	0.09	1347.3	0.4	682.9	0.2	806.52	0.40	1322.0	0.8	709.5	0.6
15.00	803.02	0.09	1327.6	0.4	706.6	0.2	802.66	0.40	1301.8	0.8	735.2	0.6
20.00	799.33	0.09	1307.9	0.4	731.4	0.3	798.79	0.41	1281.6	0.9	762.2	0.6
25.00	795.65	0.09	1288.5	0.4	757.0	0.3	794.90	0.42	1261.9	0.9	790.1	0.7
30.00	791.95	0.09	1269.3	0.4	783.8	0.3	791.00	0.43	1242.1	0.9	819.4	0.7
35.00	788.25	0.09	1250.2	0.4	811.6	0.3	787.08	0.44	1222.7	0.9	849.9	0.8
40.00	784.53	0.09	1231.3	0.4	840.8	0.3						
45.00	780.81	0.09	1212.5	0.4	871.1	0.3						
50.00	777.07	0.09	1194.0	0.4	902.7	0.3						

[a]Ambient pressure during measurements was ~83 kPa. [b]$U(\overline{\rho})$, $U(\overline{w})$, and $U(\overline{\kappa}_s)$ are expanded uncertainties at the 95% confidence level for density, speed of sound, and adiabatic compressibility, respectively.

thermally stressed samples are shown in Figure 1 along with the previously discussed results for the two unstressed fuels. The results indicate that both RP-1 and RP-2 experienced similar changes in composition when thermally stressed, with the largest changes observed for paraffins and alkylbenzenes. More specifically, the paraffin concentration for RP-1 decreased from 35% for the unstressed fuel to 33% for RP-1-TS-475 and to 22% for RP-1-TS-510. For RP-2, the paraffin concentration decreased from 34% to 30% for RP-2-TS-475 and to 23% for RP-2-TS-510. The alkylbenzene concentration for both fuels remained relatively constant after thermal stressing at 475 °C but increased quite dramatically after stressing at 510 °C, going from 7% to 16% for RP-1 and from 4% to 11% for RP-2. Overall, both fuels showed decomposition to smaller, more volatile molecules with the degree of decomposition increasing significantly after thermal stressing at 510 °C compared to 475 °C.

As a consequence of the observed decomposition, thermal stressing generated a significant gaseous fraction for both fuels, constituting approximately 30% and 50% (mass/mass) of products at 475 and 510 °C, respectively.[29] The gaseous and liquid phases were separated and their compositions independently analyzed. Phase separation was achieved using a specially designed two-phase separator collection manifold described in detail elsewhere.[29,41] The preceding discussion of composition referred to the separate liquid phase; the gas phase was found to contain hydrogen, carbon monoxide, methane, ethane, oxygen, and nitrogen, as well as hydrocarbons as large as methyl butane.[29] Even after phase separation, the stressed liquids still contained dissolved and entrained gaseous species. To minimize the potential for component loss from off-gassing during storage, the thermally stressed liquids were stored in tightly sealed bottles at approximately 5 °C.

2.2. Thermophysical Property Measurements. A commercial density and sound speed analyzer was used to simultaneously measure these two properties over the combined temperature range 5 to 50 °C and at ambient pressure (~83 kPa in Boulder, CO). The speed of sound is measured using a time-of-flight technique. The sound speed cell consists of a circular cylindrical cavity (8 mm diameter and 5 mm thick) that is sandwiched between two piezoelectric ultrasound transducers. One transducer sends sound pulses through the sample-filled cavity at a frequency of approximately 3 MHz, and the speed of sound (w) is ultimately determined by measuring the time it takes for those pulses to reach the second transducer. The densimeter employs the vibrating-tube method where density (ρ) is derived from the resonant frequency of a sample-filled U-shaped tube as it vibrates perpendicular to its plane in an electromagnetic field. The resonator in this instrument is constructed of borosilicate glass. The sound speed cell and density cell are both housed in a thermostated copper block whose temperature is controlled between 5 and 70 °C with a combination of thermoelectric Peltier elements and an integrated Pt-100 resistance thermometer. Measurements of air and water performed at 20, 40, and 60 °C are required to adjust the apparatus constants in the instrument's working equations for both sound speed and density; this is referred to as an adjustment procedure. Additionally, regular calibration measurements are performed to verify the instrument's performance between adjustment procedures. Our calibration procedure involves measuring water and toluene standard reference material (SRM) 211d every 5 °C from 70 to 5 °C. Additional details about the density and sound speed analyzer can be found in Fortin et al.[42] and Laesecke et al.[43]

A commercial viscodensimeter was used to simultaneously measure viscosity and density over the combined temperature range −10 to 50 °C and at ambient pressure. Density is measured with a vibrating-tube densimeter made of borosilicate glass. Viscosity is measured with a Stabinger rotating concentric cylinder viscometer. The horizontally mounted outer cylinder is made of Hastelloy, while the inner cylinder is made of titanium. The inner cylinder contains a small magnet but is otherwise hollow. When sample is injected into the cell, it fills the annular gap between the inner and the outer cylinders. During measurements, the outer cylinder is rotated at 3500 rpm by an external electric motor and the inner cylinder is dragged into rotation by the rotating sample liquid. The revolutions of the rotating field of the magnet in the inner cylinder are measured with a Hall effect sensor, and the dynamic viscosity (η) is ultimately obtained from the ratio of the number of revolutions of the outer and inner cylinders. Both the density and the viscosity measurement cells are housed in a thermostated copper block whose temperature is controlled between 0 and 100 °C with a combination of thermoelectric Peltier elements and an integrated Pt-100 resistance thermometer. The addition of an external circulating bath extends the instrument's temperature range down to −10 °C. Measurements of a series of certified standards spanning the viscosity and density range of the instrument are required at 20, 60, and 100 °C and at 20, 40, 60, 80, and 100 °C to adjust the apparatus constants in the instrument's working equations for viscosity and density, respectively. Additional details about the viscodensimeter can be found in Laesecke et al.[43]

With both instruments, sample liquid is injected into the instrument using a disposable syringe. Approximately 3 mL of sample is sufficient to fill both measurement cells (sound speed and density, or density and viscosity, depending on the specific instrument). Measurements were made via programmed scans between the minimum and maximum temperature in 5 °C increments. The maximum temperatures for the thermally stressed samples were 50 °C for the TS-475 samples and 35 °C for the TS-510 samples; the aforementioned entrained gaseous species in the thermally stressed samples would result in the formation of interfering gas bubbles in the measurement cells at higher temperatures. Multiple measurement scans were performed for each of the thermally stressed samples with a fresh aliquot of sample fluid injected into the instrument prior to the start of each scan. For measurements made with the density and sound speed

Table 2. Measured Densities and Speeds of Sound and Derived Adiabatic Compressibilities for Thermally Stressed RP-2 at Ambient Pressure[a]

	RP-2-TS-475						RP-2-TS-510					
t (°C)	$\overline{\rho}$ (kg m^{-3})	$U(\overline{\rho})^b$ (kg m^{-3})	$\overline{w}$ (m s^{-1})	$U(\overline{w})^b$ (m s^{-1})	$\overline{\kappa}_s$ (TPa^{-1})	$U(\overline{\kappa}_s)^b$ (TPa^{-1})	$\overline{\rho}$ (kg m^{-3})	$U(\overline{\rho})^b$ (kg m^{-3})	$\overline{w}$ (m s^{-1})	$U(\overline{w})^b$ (m s^{-1})	$\overline{\kappa}_s$ (TPa^{-1})	$U(\overline{\kappa}_s)^b$ (TPa^{-1})
5.00	810.71	0.09	1367.0	0.5	660.1	0.2	807.21	0.18	1339.0	0.5	691.0	0.3
10.00	807.03	0.09	1346.8	0.5	683.2	0.3	803.35	0.18	1318.3	0.5	716.2	0.3
15.00	803.35	0.09	1326.7	0.5	707.2	0.3	799.49	0.19	1297.9	0.5	742.5	0.4
20.00	799.66	0.09	1306.9	0.5	732.2	0.3	795.62	0.19	1277.7	0.6	770.0	0.4
25.00	795.97	0.10	1286.9	0.5	758.6	0.3	791.73	0.19	1257.5	0.6	798.7	0.4
30.00	792.28	0.09	1267.4	0.5	785.8	0.3	787.83	0.19	1237.7	0.6	828.6	0.5
35.00	788.57	0.09	1248.1	0.5	814.1	0.4	783.87	0.19	1218.1	0.7	860.0	0.5
40.00	784.85	0.09	1229.0	0.6	843.6	0.4						
45.00	781.12	0.10	1210.1	0.6	874.2	0.4						
50.00	777.40	0.10	1191.3	0.6	906.4	0.5						

[a]Ambient pressure during measurements was ~83 kPa. [b]$U(\overline{\rho})$, $U(\overline{w})$, and $U(\overline{\kappa}_s)$ are expanded uncertainties at the 95% confidence level for density, speed of sound, and adiabatic compressibility, respectively.

analyzer, seven replicate scans were performed for each sample, and at least five replicate measurement scans were performed for measurements made with the viscodensimeter. In between samples, the measurement cells in both instruments were thoroughly cleaned and dried to ensure that cross-contamination did not occur.

3. RESULTS AND DISCUSSION

3.1. Density. Results of the density measurements made with the density and sound speed analyzer are presented in Tables 1 and 2; Table 1 contains data for thermally stressed RP-1, and Table 2 contains data for thermally stressed RP-2. For each sample, the tabulated densities represent the average ($\overline{\rho}$) of seven replicate measurement scans. Also included in the tables are the associated expanded uncertainty estimates ($U(\overline{\rho})$). The expanded uncertainty is calculated using the expression

$$U(\overline{\rho}) = t_p(df_\rho)\cdot u(\overline{\rho}) \quad (1)$$

where $t_p(df_\rho)$ is taken from the t distribution for df_ρ degrees of freedom and a p percent level of confidence (typically 95%) and $u(\overline{\rho})$ is the combined standard uncertainty for the averaged density measurements. The corresponding value of $t_p(df_\rho)$ can be found in table G.2 of the *Guide to the Expression of Uncertainty in Measurement*[44] by interpolation or by truncating df_ρ to the next lower integer. Additional details concerning the uncertainty analysis calculations can be found in Fortin et al.[42] For the RP-1 samples (Table 1), $t_p(df_\rho)$ ranged from 2.01 to 2.45 and the reported absolute expanded uncertainties (0.09−0.44 kg m^{-3}) correspond to relative expanded uncertainties of 0.01−0.06%. For the RP-2 samples (Table 2), $t_p(df_\rho)$ ranged from 2.07 to 2.31 and the reported absolute expanded uncertainties (0.09−0.19 kg m^{-3}) correspond to relative expanded uncertainties of 0.01−0.02%.

The averaged densities shown in Tables 1 and 2 are plotted as a function of temperature in Figure 2. Data for RP-1 are shown in the top portion of the figure, and data for RP-2 are shown below. Also shown in Figure 2 are previously reported[32] ambient pressure (~83 kPa) density measurements for unstressed RP-1 and RP-2. These data were measured with the same density and sound speed analyzer used in this work. They have been included to demonstrate how the changes in composition that result from thermal stressing are reflected in the observed density behavior of the fuels. The overlap in data between the thermally stressed and unstressed samples is somewhat limited as a result of the previously mentioned lower maximum measurement temperatures for the thermally stressed samples.

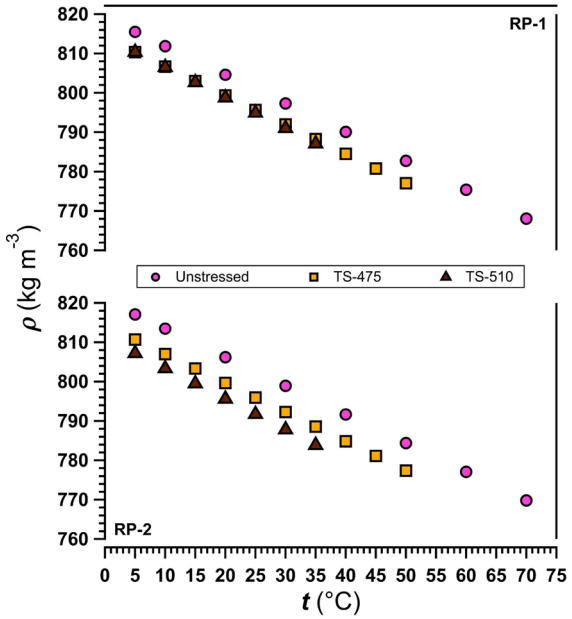

Figure 2. Ambient pressure density measurements for thermally stressed RP-1 and RP-2 samples plotted as a function of temperature. The top half of the graph contains data for RP-1; RP-2 data are shown below. Results from earlier measurements[32] of the two unstressed fuels have been included for comparison. The earlier measurements were made using the same density and sound speed analyzer used in the current work.

The first feature that is apparent when looking at Figure 2 is that the densities of the two unstressed fuels are very similar. RP-1 has densities ranging from 768.09 to 815.50 kg m^{-3}, while RP-2 has densities ranging from 769.80 to 817.10 kg m^{-3},[32] a difference of approximately 0.2%. The similarities in density are not particularly surprising given the aforementioned similarities in composition between the two unstressed fuels (Figure 1). The second feature that is readily apparent from Figure 1 is that, for both RP-1 and RP-2, the densities of the thermally stressed samples are lower relative to their respective unstressed samples, but the magnitudes of those decreases in density are different for the two fuels. For RP-1, the two thermally stressed

dx.doi.org/10.1021/ef400193d | Energy Fuels 2013, 27, 2506−2514

samples have similar densities, differing from one another by only 0.001% at 5 °C and 0.1% at 35 °C. As a result, relative to unstressed RP-1, RP-1-TS-475 has densities that are 0.6−0.7% lower, while RP-1-TS-510 has densities that are 0.6−0.8% lower. For both samples, the deviation from unstressed RP-1 values increases with increasing temperature. In contrast to RP-1, the thermally stressed RP-2 samples exhibit densities that are more significantly different from one another, varying by 0.4% at 5 °C and 0.6% at 35 °C. Consequently, relative to unstressed RP-2, RP-2-TS-475 has densities that are 0.8−0.9% lower and RP-2-TS-510 has densities that are 1.2−1.4% lower. As was the case with the RP-1 samples, the deviations relative to unstressed RP-2 densities increase with increasing temperature.

The observed decrease in density resulting from thermal stressing is not entirely unexpected. As was previously discussed, as RP-1 and RP-2 decompose, the concentrations of smaller, more volatile molecules increase. One might expect density to decrease as the concentrations of small hydrocarbons increase relative to the concentrations of large hydrocarbons. For example, *n*-dodecane has a density of 745.73 kg m^{-3} at 25 °C and 0.1 MPa,[45] whereas *n*-pentane has a density of 620.83 kg m^{-3} at the same conditions;[46] the former was found to be present in all six samples being discussed here, while the latter was present only in the thermally stressed samples, excluding RP-2-TS-475. Obviously this very crude example does not consider that the fluids in question are extremely complex and not simple mixtures of straight-chain alkanes; it is simply provided to illustrate why, ostensibly, one might expect more small hydrocarbons to result in a lower density. The observed trend in densities is also consistent with what one would expect when dissolved gaseous species are present; as was previously mentioned, the concentration of these species was shown to increase from unstressed to TS-475 to TS-510.[29]

3.2. Speed of Sound. Results of the speed of sound measurements are also presented in Tables 1 and 2; Table 1 contains data for thermally stressed RP-1, and Table 2 contains data for thermally stressed RP-2. Included in the table are averages ($\overline{w}$) for the seven replicate measurement scans performed for each sample and the associated expanded uncertainty estimates ($U(\overline{w})$). Expanded uncertainties for sound speed measurements were calculated using a method analogous to that previously described for density measurements; additional details can be found in Fortin et al.[42] For the sound speed data reported in Table 1, $t_p(df_w)$ ranged from 1.99 to 2.23, and the absolute expanded uncertainties (0.4−0.9 m s^{-1}) correspond to relative expanded uncertainties of 0.03−0.07%. For the data reported in Table 2, $t_p(df_w)$ ranged from 1.99 to 2.10 and reported absolute expanded uncertainties (0.5−0.7 m s^{-1}) correspond to relative expanded uncertainties of 0.03−0.06%.

The averaged sound speeds shown in Tables 1 and 2 are plotted as a function of temperature in Figure 3. Data for RP-1 are shown in the top portion of the figure, and data for RP-2 are shown below. Also shown in Figure 3 are previously reported[32] ambient pressure (~83 kPa) sound speed measurements for unstressed RP-1 and RP-2. It is clear from Figure 3 that, as was the case with density, the sound speeds of the two unstressed fuels are very similar. RP-1 has speeds of sound ranging from 1135.6 to 1381.3 m s^{-1}, while RP-2 ranges from 1138.2 to 1383.3 m s^{-1},[32] a difference of, at most, 0.2%. Again, the similarities in sound speed are not surprising given the similarities in composition (Figure 1). It is also apparent from Figure 3 that the sound speeds of the thermally stressed

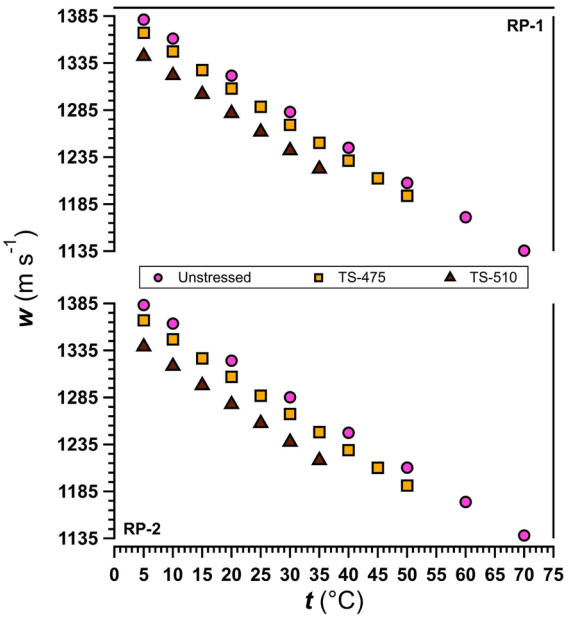

Figure 3. Ambient pressure speed of sound measurements for thermally stressed RP-1 and RP-2 samples plotted as a function of temperature. The top half of the graph contains data for RP-1; RP-2 data are shown below. Results from earlier measurements[32] of the two unstressed fuels have been included for comparison. The earlier measurements were made using the same density and sound speed analyzer used in the current work.

samples are lower relative to their respective unstressed samples for both RP-1 and RP-2. For RP-1, in contrast to what was observed with density (Figure 2), RP-1-TS-475 and RP-1-TS-510 exhibit markedly different sound speeds from one another with RP-1-TS-510 showing values that are 1.8% lower at 5 °C and 2.2% lower at 35 °C. Consequently, RP-1-TS-475 has sound speeds that are 1.0−1.1% lower than unstressed RP-1, whereas RP-1-TS-510 has sound speeds that are 2.8−3.2% lower. For both RP-1 thermally stressed samples, the magnitude of deviation relative to the unstressed fuel increases with increasing temperature. For RP-2, the thermally stressed samples have sound speeds that differ from one another by 2.0% at 5 °C and 2.4% at 35 °C. Relative to unstressed RP-2, RP-2-TS-475 has sound speeds that are 1.2−1.6% lower and RP-2-TS-510 has sound speeds that are 3.2−3.7% lower. Once again, the magnitudes of these deviations increase with increasing temperature.

3.3. Adiabatic Compressibility. Using the measured densities and speeds of sound presented in Tables 1 and 2, adiabatic compressibilities (κ_s) were calculated via the thermodynamic relationship

$$\kappa_s = \frac{1}{\rho \cdot w^2} \tag{2}$$

where ρ is the density, w is the speed of sound, and the subscript s indicates "at constant entropy". Results of these calculations are included in their respective tables, Table 1 for RP-1 samples and Table 2 for RP-2 samples. Tabulated values are the averages ($\overline{\kappa}_s$) of seven replicate measurement scans of density and speed of sound and the associated expanded uncertainty estimates ($U(\overline{\kappa}_s)$). Because the adiabatic compressibility is derived from two measured quantities, the expanded relative uncertainties associated with density and speed of sound were combined in quadrature to determine the expanded

dx.doi.org/10.1021/ef400193d | Energy Fuels 2013, 27, 2506−2514

uncertainties reported in Tables 1 and 2. The reported absolute expanded uncertainties for RP-1 (0.2−0.8 TPa^{-1}) correspond to relative expanded uncertainties of 0.03−0.09%. For RP-2, reported absolute expanded uncertainties (0.2−0.5 TPa^{-1}) correspond to relative expanded uncertainties of 0.04−0.06%.

The averaged adiabatic compressibilities shown in Tables 1 and 2 are plotted as a function of temperature in Figure 4. Data

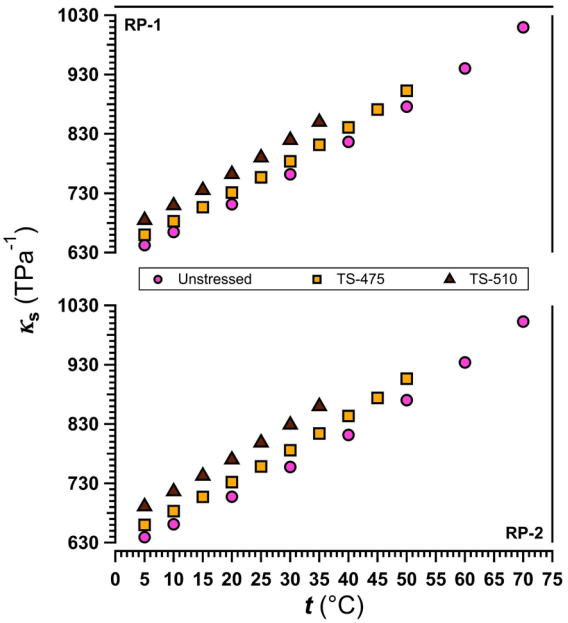

Figure 4. Calculated ambient pressure adiabatic compressibilities for thermally stressed RP-1 and RP-2 samples plotted as a function of temperature. The top half of the graph contains data for RP-1; RP-2 data are shown below. Results from earlier measurements[32] of the two unstressed fuels have been included for comparison. The earlier measurements were made using the same density and sound speed analyzer used in the current work.

for RP-1 are shown in the top portion of the figure, and data for RP-2 are shown below. Also shown in Figure 4 are previously reported[32] ambient pressure (~83 kPa) adiabatic compressibility data for unstressed RP-1 and RP-2. As expected, the adiabatic compressibilities of the two unstressed fuels are similar, albeit less so than was the case for density and speed of sound; RP-1 ranges from 642.67 to 1009.7 TPa^{-1}, while RP-2 ranges from 639.19 to 1002.8 TPa^{-1},[32] a difference of, at most, 0.7%. For both RP-1 and RP-2, the adiabatic compressibilities of the thermally stressed samples are higher relative to their respective unstressed samples. Specifically, RP-1-TS-475 has adiabatic compressibilites that are 2.7−3.1% higher than unstressed RP-1, whereas RP-1-TS-510 has values that are 6.6−7.5% higher. Relative to unstressed RP-2, RP-2-TS-475 has adiabatic compressibilities that are 3.3−4.1% higher and RP-2-TS-510 has values that are 8.1−9.4% higher. For both RP-1 and RP-2, the deviations of the thermally stressed samples relative to their respective unstressed samples increase with increasing temperature.

3.4. Viscosity. Results of the dynamic viscosity measurements made with the viscodensimeter for the four thermally stressed samples are presented in Table 3. For each sample, the tabulated dynamic viscosities represent the average ($\overline{\eta}$) of at least five replicate measurement scans. Also included in the table are the associated expanded uncertainty estimates ($U(\overline{\eta})$), which were calculated using a method analogous to that previously described for density and speed of sound measurements; additional details can be found in Fortin et al.[42] and Laesecke et al.[43] For the dynamic viscosity measurements reported in Table 3, $t_p(df_\eta)$ ranged from 2.12 to 2.78. The reported absolute expanded uncertainties (0.008−0.0328 mPa s) correspond to relative expanded uncertainties of 0.3−3.9%.

The averaged dynamic viscosities shown in Table 3 are plotted as a function of temperature in Figure 5 with data for RP-1 shown in the top portion of the figure and data for RP-2 shown below. Also shown in Figure 5 are previously reported[32] ambient pressure (~83 kPa) dynamic viscosity data for unstressed RP-1 and RP-2. In contrast to the current measurements of the thermally stressed samples, Outcalt et al.[32] used an automated open gravitational flow viscometer to measure the kinematic viscosity of the unstressed fuels; those measurements were then combined with their density measurements from the density and sound speed analyzer to calculate the reported dynamic viscosity values (see eq 3 below). Note that the overlap of viscosity data between the thermally stressed and unstressed samples is reduced to four data points for the TS-475 samples and to just two data points for the TS-510

Table 3. Measured Dynamic Viscosities for Thermally Stressed RP-1 and RP-2 at Ambient Pressure[a]

	RP-1-TS-475		RP-1-TS-510		RP-2-TS-475		RP-2-TS-510	
t (°C)	$\overline{\eta}$ (mPa s)	$U(\overline{\eta})^b$ (mPa s)	$\overline{\eta}$ (mPa s)	$U(\overline{\eta})^b$ (mPa s)	$\overline{\eta}$ (mPa s)	$U(\overline{\eta})^b$ (mPa s)	$\overline{\eta}$ (mPa s)	$U(\overline{\eta})^b$ (mPa s)
−10.00	2.903	0.008	1.840	0.013	2.952	0.021	1.889	0.026
−5.00	2.554	0.010	1.655	0.014	2.592	0.019	1.699	0.024
0.00	2.263	0.009	1.499	0.013	2.293	0.019	1.536	0.024
5.00	2.021	0.009	1.363	0.013	2.047	0.015	1.400	0.019
10.00	1.816	0.010	1.246	0.014	1.839	0.015	1.280	0.016
15.00	1.643	0.010	1.147	0.011	1.660	0.014	1.175	0.016
20.00	1.495	0.012	1.058	0.011	1.511	0.011	1.086	0.010
25.00	1.366	0.013	0.9797	0.0088	1.379	0.011	1.003	0.011
30.00	1.253	0.013	0.9026	0.0172	1.266	0.010	0.9142	0.0198
35.00	1.154	0.014	0.8387	0.0127	1.167	0.008	0.8407	0.0328
40.00	1.069	0.012			1.078	0.009		
45.00	0.9956	0.0131			0.9993	0.0104		
50.00	0.9225	0.0132			0.9277	0.0143		

[a]Ambient pressure during measurements was ~83 kPa. [b]$U(\overline{\eta})$ is expanded uncertainty at the 95% confidence level for dynamic viscosity.

dx.doi.org/10.1021/ef400193d | Energy Fuels 2013, 27, 2506−2514

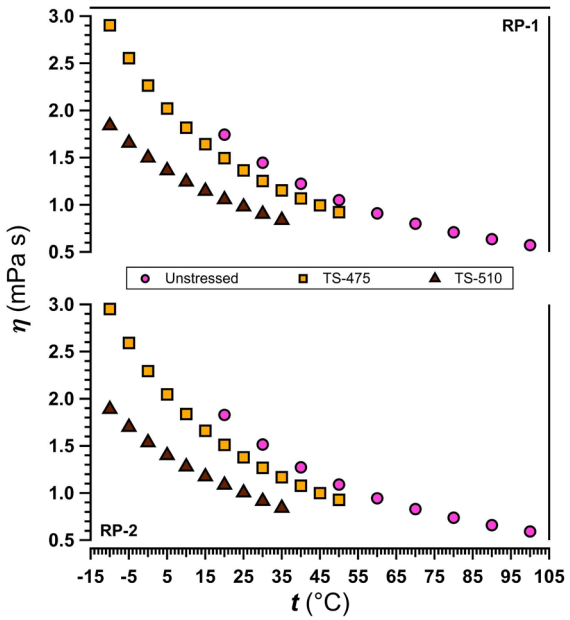

Figure 5. Ambient pressure dynamic viscosity measurements for thermally stressed RP-1 and RP-2 samples plotted as a function of temperature. The top half of the graph contains data for RP-1; RP-2 data are shown below. Results from earlier measurements[32] of the two unstressed fuels have been included for comparison. The unstressed values were derived from separate kinematic viscosity and density measurements. Kinematic viscosity was measured using a different viscometer from that used in the current work. Density was measured using the same density and sound speed analyzer used in the current work.

samples. This is because, in addition to the previously mentioned upper temperature limits for the thermally stressed samples, the automated open gravitational flow viscometer used by Outcalt et al.[32] to measure the unstressed samples is limited to a lower temperature of 20 °C.

The dynamic viscosities of the two unstressed fuels are fairly similar; RP-1 ranges from 0.5727 to 1.743 mPa s, while RP-2 ranges from 0.5918 to 1.828 mPa s,[32] a difference of, at most, 4.9%. For both RP-1 and RP-2, the dynamic viscosities of the thermally stressed samples are considerably lower relative to their respective unstressed samples with the TS-510 samples showing the most significant deviations. RP-1-TS-475 values are 12.1−14.2% lower than unstressed RP-1, and RP-1-TS-510 values are 37.6−39.3% lower. Relative to unstressed RP-2, RP-2-TS-475 has dynamic viscosities that are 15.0−17.3% lower and RP-2-TS-510 has values that are 39.7−40.6% lower. In contrast to what was observed with the other properties, for both RP-1 and RP-2, the deviations of the thermally stressed samples relative to their respective unstressed samples decrease with increasing temperature.

In addition to the dynamic viscosities reported in Table 3, the viscodensimeter used in the current work automatically calculates and records kinematic viscosities (ν) via the thermodynamic relationship

$$\nu = \frac{\eta}{\rho} \tag{3}$$

where η and ρ are the measured dynamic viscosity and density at each temperature. Those kinematic viscosity results are presented in Table 4 for the four thermally stressed samples. As with the other properties, included in the table are the averages ($\overline{\nu}$) of at least five replicate measurement scans and the associated expanded uncertainty estimates ($U(\overline{\nu})$). Because the kinematic viscosity is derived from two measured quantities, the expanded relative uncertainties associated with dynamic viscosity and density were combined in quadrature to determine the expanded uncertainties reported in Table 4. The reported absolute expanded uncertainties (0.010−0.042 mm^2 s^{-1}) correspond to relative expanded uncertainties of 0.3−3.9%.

The averaged kinematic viscosities shown in Table 4 are plotted as a function of temperature in Figure 6. Data for RP-1 are shown in the top portion of the figure, and data for RP-2 are shown below. Previously reported[32] ambient pressure (~83 kPa) kinematic viscosity data for unstressed RP-1 and RP-2 are also shown in Figure 6. As was previously mentioned, Outcalt et al.[32] used an automated open gravitational flow viscometer to measure the kinematic viscosity directly, and the lower temperature limit of that instrument is 20 °C. The kinematic viscosities of the two unstressed fuels are within 3.1% and 4.7% of each other; RP-1 ranges from 0.7678 to 2.166 mm^2 s^{-1}, while RP-2 ranges from 0.7916 to 2.267 mm^2 s^{-1}.[32] Once again, for

Table 4. Measured Kinematic Viscosities for Thermally Stressed RP-1 and RP-2 at Ambient Pressure[a]

	RP-1-TS-475		RP-1-TS-510		RP-2-TS-475		RP-2-TS-510	
t (°C)	$\overline{\nu}$ (mm^2 s^{-1})	$U(\overline{\nu})^b$ (mm^2 s^{-1})	$\overline{\nu}$ (mm^2 s^{-1})	$U(\overline{\nu})^b$ (mm^2 s^{-1})	$\overline{\nu}$ (mm^2 s^{-1})	$U(\overline{\nu})^b$ (mm^2 s^{-1})	$\overline{\nu}$ (mm^2 s^{-1})	$U(\overline{\nu})^b$ (mm^2 s^{-1})
−10.00	3.533	0.010	2.241	0.016	3.590	0.026	2.307	0.032
−5.00	3.122	0.012	2.026	0.017	3.166	0.024	2.084	0.030
0.00	2.779	0.012	1.844	0.016	2.814	0.023	1.894	0.030
5.00	2.492	0.012	1.685	0.016	2.524	0.019	1.734	0.024
10.00	2.250	0.012	1.547	0.018	2.277	0.018	1.593	0.020
15.00	2.045	0.013	1.431	0.013	2.066	0.018	1.470	0.020
20.00	1.870	0.015	1.326	0.014	1.889	0.014	1.365	0.013
25.00	1.716	0.016	1.234	0.011	1.731	0.014	1.267	0.014
30.00	1.581	0.017	1.143	0.022	1.598	0.012	1.161	0.025
35.00	1.463	0.018	1.067	0.016	1.480	0.010	1.073	0.042
40.00	1.362	0.015			1.373	0.011		
45.00	1.275	0.017			1.279	0.013		
50.00	1.187	0.017			1.193	0.018		

[a]Ambient pressure during measurements was ~83 kPa. [b]$U(\overline{\nu})$ is expanded uncertainty at the 95% confidence level for kinematic viscosity.

dx.doi.org/10.1021/ef400193d | Energy Fuels 2013, 27, 2506−2514

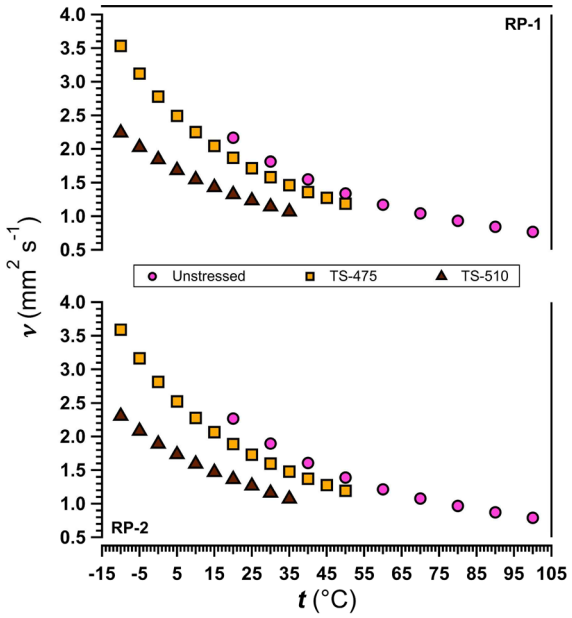

Figure 6. Ambient pressure kinematic viscosity measurements for thermally stressed RP-1 and RP-2 samples plotted as a function of temperature. The top half of the graph contains data for RP-1; RP-2 data are shown below. Results from earlier measurements[32] of the two unstressed fuels have been included for comparison. The earlier measurements were made using an apparatus different from that used in the current work.

both RP-1 and RP-2, the kinematic viscosities of the thermally stressed samples are considerably lower relative to their respective unstressed samples, with the TS-510 samples drastically so. Specifically, RP-1-TS-475 kinematic viscosities are 11.5−13.7% lower than unstressed RP-1, while those for RP-1-TS-510 are 37.0−38.8% lower. Similarly, RP-2-TS-475 has kinematic viscosities that are 14.2−16.7% lower than unstressed RP-2, and RP-2-TS-510 has values that are 38.8−39.8% lower. The deviations of the thermally stressed samples relative to their respective unstressed samples decrease with increasing temperature.

4. CONCLUSIONS

In this work, thermophysical property measurements for thermally stressed rocket propellants RP-1 and RP-2 have been presented. A total of four fuel samples were measured in this work; they comprised two different samples, stressed at two different temperatures (475 and 510 °C), for each of the two rocket propellants. Ambient pressure density and speed of sound data, along with the derived property of adiabatic compressibility, were reported over the temperature range of 5−50 °C for the two samples stressed at 475 °C and over the range of 5−35 °C for the two samples stressed at 510 °C. In addition, ambient pressure dynamic and kinematic viscosities over the temperature ranges from −10 to 50 °C and −10 to 35 °C were reported for the samples stressed at 475 and 510 °C, respectively. Data for the thermally stressed samples were also compared to previously reported measurements[32] of their respective unstressed fuels. Previous work by Windom and Bruno[29] demonstrated that thermal stressing of both RP-1 and RP-2 resulted in increased concentrations of small, more volatile, molecules, and higher stressing temperatures resulted in greater decomposition. These changes in composition are manifested in all of the current thermophysical property measurements as lower values for the thermally stressed samples relative to the respective unstressed fuel. Furthermore, for both fuels the TS-510 samples exhibited lower values than the TS-475 samples for all measured properties. In other words, for both RP-1 and RP-2, density, speed of sound, and viscosity decreased with increased thermal decomposition. Density showed the smallest changes relative to the unstressed fuels with percent decreases of 0.6−0.8% for RP-1 and 0.8−1.4% for RP-2. Speed of sound showed somewhat larger percent decreases of 1.0−3.2% for RP-1 and 1.2−3.7% for RP-2. Dynamic viscosity showed the largest changes with percent decreases of 12.1−39.3% for RP-1 and 15.0−40.6% for RP-2. Since adiabatic compressibility is inversely proportional to the two measured properties of density and speed of sound (see eq 2), the observed trend was reversed; increased thermal decomposition resulted in increased values for both RP-1 and RP-2. Specifically, adiabatic compressibility exhibited percent increases of 2.7−7.5% and 3.3−9.4% for RP-1 and RP-2, respectively. In all instances, RP-2 showed greater changes as a result of thermal decomposition than did RP-1.

AUTHOR INFORMATION

Corresponding Author

*Phone: 303-497-3522. Fax: 303-497-6682. E-mail: tfortin@boulder.nist.gov.

Notes

The authors declare no competing financial interest.

ACKNOWLEDGMENTS

Financial support of the Air Force Research Laboratory (MIPR F1SBAA0138G001) is gratefully acknowledged. Contribution of the National Institute of Standards and Technology. Not subject to Copyright in the U.S.A.

REFERENCES

(1) Sutton, G. P. History of Liquid Propellant Rocket Engines in the United States. *J. Propul. Power* **2003**, *19*, 978−1007.

(2) Edwards, T. Liquid Fuels and Propellants for Aerospace Propulsion: 1903−2003. *J. Propul. Power* **2003**, *19*, 1089−1107.

(3) Huzel, D. K.; Hwang, D. H. *Modern Engineering for Design of Liquid-Propellant Rocket Engines*; American Institute of Aeronautics and Astronautics: Washington, DC, 1992.

(4) Salakhutdinov, G. M. Development of Methods of Cooling Liquid Propellant Rocket Engines (ZhRDs), 1903−1970. In *History of Rocketry and Astronautics*; Skoog, Å. I., Ed.; American Astronautical Society: San Diego, CA, 1990; pp 115−122.

(5) Detail Specification Propellant, Rocket Grade Kerosene, MIL-DTL-25576E; April 14, 2006.

(6) Ziebland, H.; Parkinson, R. C. *Heat Transfer in Rocket Engines*, AGARD-AG-148-71; North Atlantic Treaty Organization, Advisory Group for Aerospace Research and Development: Neuilly-sur-Seine, France, 1971.

(7) Van Huff, N. E. *Liquid Rocket Engine Fluid-Cooled Combustion Chambers*, NASA-SP-8087; National Aeronautics and Space Administration, Lewis Research Center: Cleveland, OH, 1972.

(8) Wagner, W. R.; Shoji, J. M. Advanced Regenerative Cooling Techniques for Future Space Transportation Systems. *11th AIAA/SAE Joint Propulsion Conference*, Anaheim, CA, Sept. 29−Oct. 1, 1975; AIAA Paper 75-1247.

(9) Wheeler, D. B. *Tripropellant Engine Study*, NASA-CR-150444; National Aeronautics and Space Administration, Marshall Space Flight Center: Huntsville, AL, 1977.

(10) Cook, R. T.; Quentmeyer, R. J. Advanced Cooling Techniques for High Pressure Hydrocarbon-Fueled Rocket Engines. *16th AIAA/*

ASME/SAE Joint Propulsion Conference, Hartford, CT, Jun. 30−Jul. 2, 1980; AIAA Paper 80-1266.
(11) Roback, R.; Szetela, E. J.; Spadaccini, L. J. *Deposit Formation in Hydrocarbon Rocket Fuels-Executive Summary Report*, NASA-CR-165492; National Aeronautics and Space Administration, Lewis Research Center: Cleveland, OH, 1981.
(12) Michel, R. W. *Combustion Performance and Heat Transfer Characterization of LOX/Hydrocarbon Type Propellants*, NASA-CR-171712; National Aeronautics and Space Administration, Johnson Space Center: Houston, TX, 1983.
(13) Giovanetti, A. J.; Spadaccini, L. J.; Szetela, E. J. *Deposit Formation and Heat Transfer in Hydrocarbon Rocket Fuels*, NASA-CR-168277; National Aeronautics and Space Administration, Lewis Research Center: Cleveland, OH, 1983.
(14) Rosenberg, S. D.; Gage, M. L. Compatibility of Hydrocarbon Fuels with Booster Engine Combustion-Chamber Liners. *J. Propul. Power* **1991**, *7*, 922−928.
(15) Wohlwend, K.; Maurice, L. Q.; Edwards, T.; Striebich, R. C.; Vangsness, M.; Hill, A. S. Thermal Stability of Energetic Hydrocarbon Fuels for Use in Combined Cycle Engines. *J. Propul. Power* **2001**, *17*, 1258−1262.
(16) Stiegemeier, B.; Meyer, M. L.; Taghavi, R. A. Thermal Stability and Heat Transfer Investigation of Five Hydrocarbon Fuels: JP-7, JP-8, JP-8 + 100, JP-10, and RP-1. *38th AIAA/ASME/SAE/ASEE Joint Propulsion Conference & Exhibit*, Indianapolis, IN, Jul. 7−10, 2002; AIAA Paper 2002-3873.
(17) Bates, R.; Edwards, T.; Meyer, M. L. Heat Transfer and Deposition Behavior of Hydrocarbon Rocket Fuels. *41st AIAA Aerospace Sciences Meeting & Exhibit*, Reno, NV, Jan. 6−9, 2003; AIAA Paper 2003-123.
(18) Irvine, S. A.; Schoettmer, A. K.; Bates, R. W.; Meyer, M. L. History of Sulfur Content Effects on the Thermal Stability of RP-1 Under Heated Conditions. *40th AIAA/ASME/SAE/ASEE Joint Propulsion Conference & Exhibit*, Fort Lauderdale, FL, Jul. 11−14, 2004; AIAA Paper 2004-3879.
(19) Andersen, P. C.; Bruno, T. J. Thermal Decomposition Kinetics of RP-1 Rocket Propellant. *Ind. Eng. Chem. Res.* **2005**, *44*, 1670−1676.
(20) Meyer, M. L.; Stiegemeier, B. R. *A Materials Compatibility and Thermal Stability Analysis of Common Hydrocarbon Fuels*; National Aeronautics and Space Administration, Glenn Research Center: Cleveland, OH, 2005.
(21) Stiegemeier, B. R.; Meyer, M. L.; Driscoll, E. *RP-1 Thermal Stability and Copper Based Materials Compatibility Study*; National Aeronautics and Space Administration, Glenn Research Center: Cleveland, OH, 2005.
(22) Billingsley, M. C. Thermal Stability and Heat Transfer Characteristics of RP-2. *44th AIAA/ASME/SAE/ASEE Joint Propulsion Conference & Exhibit*, Hartford, CT, Jul. 21−23, 2008; AIAA Paper 2008-5126.
(23) Brown, S. P.; Frederick, R. A. Laboratory-Scale Thermal Stability Experiments on RP-1 and RP-2. *J. Propul. Power* **2008**, *24*, 206−212.
(24) Widegren, J. A.; Bruno, T. J. Thermal Decomposition Kinetics of Kerosene-Based Rocket Propellants. 1. Comparison of RP-1 and RP-2. *Energy Fuels* **2009**, *23*, 5517−5522.
(25) Widegren, J. A.; Bruno, T. J. Thermal Decomposition Kinetics of Kerosene-Based Rocket Propellants. 2. RP-2 with Three Additives. *Energy Fuels* **2009**, *23*, 5523−5528.
(26) Widegren, J. A.; Bruno, T. J. Thermal Decomposition Kinetics of Kerosene-Based Rocket Propellants. 3. RP-2 with Varying Concentrations of the Stabilizing Additive 1,2,3,4-Tetrahydroquinoline. *Energy Fuels* **2011**, *25*, 288−292.
(27) MacDonald, M. E.; Davidson, D. F.; Hanson, R. K. Decomposition Measurements of RP-1, RP-2, JP-7, n-Dodecane, and Tetrahydroquinoline in Shock Tubes. *J. Propul. Power* **2011**, *27*, 981−989.
(28) Van Noord, J. L.; Stiegemeier, B. R. *RP-2 Thermal Stability and Heat Transfer Investigation for Hydrocarbon Boost Engines*, NASA/TM-2010-216917; National Aeronautics and Space Administration, Glenn Research Center: Cleveland, OH, 2010.
(29) Windom, B. C.; Bruno, T. J. Assessment of the Composition and Distillation Properties of Thermally Stressed RP-1 and RP-2: Application to Fuel Regenerative Cooling. *Energy Fuels* **2011**, *25*, 5200−5214.
(30) Bruno, T. J.; Smith, B. L. Improvements in the Measurement of Distillation Curves. 2. Application to Aerospace/Aviation Fuels RP-1 and S-8. *Ind. Eng. Chem. Res.* **2006**, *45*, 4381−4388.
(31) Ott, L. S.; Hadler, A. B.; Bruno, T. J. Variability of the Rocket Propellants RP-1, RP-2, and TS-5: Application of a Composition- and Enthalpy-Explicit Distillation Curve Method. *Ind. Eng. Chem. Res.* **2008**, *47*, 9225−9233.
(32) Outcalt, S. L.; Laesecke, A.; Brumback, K. J. Thermophysical Properties Measurements of Rocket Propellants RP-1 and RP-2. *J. Propul. Power* **2009**, *25*, 1032−1040.
(33) Huber, M. L.; Lemmon, E. W.; Bruno, T. J. Effect of RP-1 Compositional Variability on Thermophysical Properties. *Energy Fuels* **2009**, *23*, 5550−5555.
(34) Huber, M. L.; Lemmon, E. W.; Ott, L. S.; Bruno, T. J. Preliminary Surrogate Mixture Models for the Thermophysical Properties of Rocket Propellants RP-1 and RP-2. *Energy Fuels* **2009**, *23*, 3083−3088.
(35) Lovestead, T. M.; Windom, B. C.; Riggs, J. R.; Nickell, C.; Bruno, T. J. Assessment of the Compositional Variability of RP-1 and RP-2 with the Advanced Distillation Curve Approach. *Energy Fuels* **2010**, *24*, 5611−5623.
(36) Standard Test Method for Hydrocarbon Types in Low Olefinic Gasoline by Mass Spectrometry. *Book of Standards*, ASTM Standard D2789-04b; American Society for Testing and Materials: West Conshohocken, PA, 2005.
(37) Smith, B. L.; Bruno, T. J. Improvements in the Measurement of Distillation Curves. 3. Application to Gasoline and Gasoline + Methanol Mixtures. *Ind. Eng. Chem. Res.* **2007**, *46*, 297−309.
(38) Bruno, T. J.; Windom, B. C. Method and Apparatus for the Thermal Stress of Complex Fluids: Application to Fuels. *Energy Fuels* **2011**, *25*, 2625−2632.
(39) Bruno, T. J.; Svoronos, P. D. N. *CRC Handbook of Fundamental Spectroscopic Correlation Charts*; Taylor and Francis CRC Press: Boca Raton, FL, 2005.
(40) Bruno, T. J.; Svoronos, P. D. N. *CRC Handbook of Basic Tables for Chemical Analysis*, 3rd ed.; Taylor and Francis CRC Press: Boca Raton, FL, 2010.
(41) Bruno, T. J. Conditioning of Flowing Multiphase Samples for Chemical Analysis. *Sep. Sci. Technol.* **2005**, *40*, 1721−1732.
(42) Fortin, T. J.; Laesecke, A.; Freund, M.; Outcalt, S. L. Advanced Calibration, Adjustment, and Operation of a Density and Sound Speed Analyzer. *J. Chem. Thermodyn.* **2013**, *57*, 276−285.
(43) Laesecke, A.; Fortin, T. J.; Splett, J. D. Density, Speed of Sound, and Viscosity Measurements of Reference Materials for Biofuels. *Energy Fuels* **2012**, *26*, 1844−1861.
(44) International Organization for Standardization (ISO). *Guide to the Expression of Uncertainty in Measurement*; ISO: Geneva, Switzerland, 1995.
(45) Lemmon, E. W.; Huber, M. L. Thermodynamic Properties of n-Dodecane. *Energy Fuels* **2004**, *18*, 960−967.
(46) Span, R. *Multiparameter Equations of State: An Accurate Source of Thermodynamic Property Data*; Springer: Berlin, Germany, 2000.